

The non-monotonicity of moist adiabatic warming

Osamu Miyawaki^a

^a *Department of Geosciences, Union College, Schenectady New York, USA*

⁴ *Corresponding author: Osamu Miyawaki, miyawako@union.edu*

5 ABSTRACT: The moist adiabat is a useful first-order approximation of the tropical stratification
6 and thus governs fundamental properties of climate such as the static stability and the lapse
7 rate feedback. While total atmospheric latent heating increases monotonically with warming,
8 the resulting change in temperature along a moist adiabat is surprisingly non-monotonic with
9 surface temperature. This phenomenon has lacked a physical explanation. This paper presents a
10 thermodynamic explanation by decomposing the sensitivity of the moist adiabatic lapse rate into
11 two competing components: 1) A Cooling Term arising from the partial derivative of saturation
12 specific humidity with respect to temperature ($\partial q_s/\partial T$), which is proportional to q_s/T^2 via the
13 Clausius-Clapeyron relation, and 2) a Pressure Term arising from the partial derivative with respect
14 to pressure ($\partial q_s/\partial p$), which is proportional to q_s/p . The non-monotonicity arises because while
15 both terms grow with temperature due to the exponential increase of saturation specific humidity
16 (q_s), the $1/T^2$ prefactor on the Cooling Term suppresses its growth more strongly than the pressure-
17 related prefactor on the Pressure Term. This mechanism also explains the non-monotonic behavior
18 of convective buoyancy and vertical velocity.

1. Introduction

The Clausius-Clapeyron relation describes the potential for a warmer atmosphere to hold more water vapor (Emanuel 1994). This principle is the basis for the positive water vapor feedback (Held and Soden 2000) and various scaling theories in response to warming including extreme precipitation (O’Gorman 2015) and CAPE (Romps 2016).

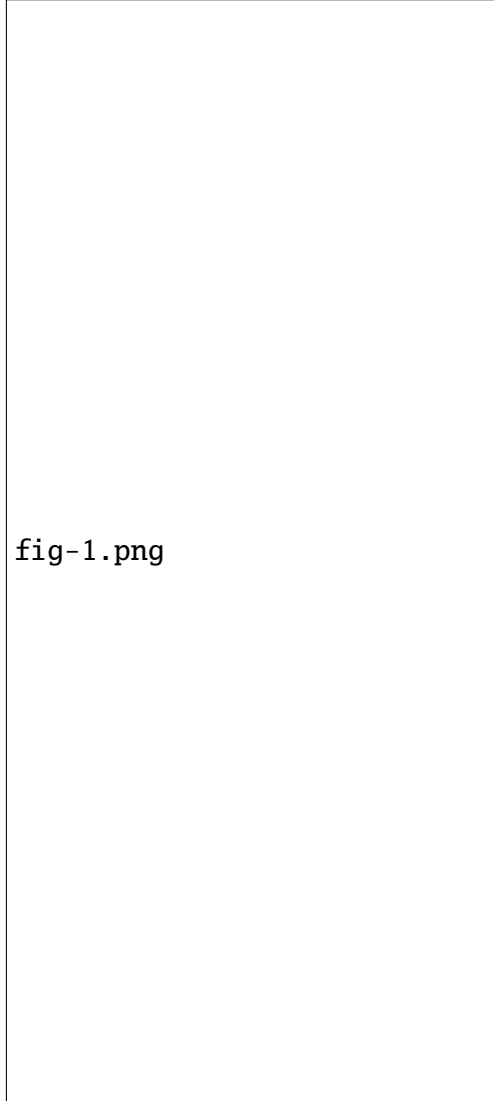
In the tropics, convection couples the surface with the free troposphere. Although processes like convective entrainment influence the details of this coupling (Miyawaki et al. 2020), moist adiabatic adjustment serves as a useful first-order approximation (Held 1993). The top-heavy warming profile predicted by moist adiabatic adjustment (Fig. 1b) is a robust feature in climate models and observations, despite historical challenges in observational records (Vallis et al. 2015; Santer et al. 2005).

This warming profile is important because it increases atmospheric static stability, which influences convection (Neelin and Held 1987). This structure also defines the tropical lapse rate feedback, a key negative feedback for global climate sensitivity (Hansen et al. 1984). The lapse rate feedback partially cancels the water vapor feedback and scales in tandem because amplified warming in the upper troposphere is a consequence of enhanced latent heat release (Held and Shell 2012). In a moist adiabatic atmosphere that is saturated at the surface, total latent heat release $L_v(q_{\text{surface}} - q_{\text{top}})$ where q_{surface} is surface specific humidity and q_{top} is the cloud top specific humidity. For deep convection that reaches the tropopause we can approximate q_{top} as $q_{\text{tropopause}}$ where $q_{\text{tropopause}}$ is invariant with surface temperature (Seeley et al. 2019). Thus to first order we expect total latent heat release to scale as q_{surface} , which increases monotonically with surface temperature following the Clausius-Clapeyron relation (Fig. 1a).

Given the monotonic increase total latent heating with surface temperature, one might expect moist adiabatic warming to also increase monotonically with surface temperature at all levels. However, it is a non-monotonic function of surface temperature at fixed pressure levels (Fig. 1c, see Appendix A for details on how the moist adiabat is calculated). This non-monotonicity arises in height coordinates (Fig. A1), with or without latent heat of fusion (see Appendix B and Fig. B1), and across different empirical formula for saturation vapor pressure (see Appendix C and Fig. C1). While Levine and Boos (2016) showed this non-monotonicity and its influence on zonal stationary

48 circulations, an explanation for the non-monotonicity in moist adiabatic warming does not exist in
49 the literature.

50 This raises the question: What physical mechanism drives this non-monotonic warming? Here
51 we provide a thermodynamic explanation for the origin of non-monotonicity in moist adiabatic
52 warming and its cascading effects on buoyancy and vertical velocity.



53 FIG. 1. (a) Surface saturation specific humidity as a function of surface temperature. (b) Vertical profiles of
54 moist adiabatic warming to a 4 K surface warming, plotted against pressure, for $T_s = 280, 290, 300, 310,$ and 320
55 K. (c) The moist adiabatic warming at 500, 400, 300, and 200 hPa as a function of surface temperature shows a
56 non-monotonic response where warming peaks at an intermediate surface temperature.

57 2. Theory of Non-Monotonic Warming

58 We start by defining the moist adiabatic temperature profile in pressure coordinates $T(p)$ in terms
59 of the moist adiabatic lapse rate $\Gamma_m = dT/dp$:

$$T(p) = T_s + \int_{p_s}^p \Gamma_m dp' \quad (1)$$

60 where T_s is surface temperature. The difference between a perturbed and baseline state (Δ) then
61 follows as

$$\Delta T(p) = \Delta T_s + \int_{p_s}^p \Delta \Gamma_m dp' \quad (2)$$

62 For a small perturbation, $\Delta \Gamma_m$ can be approximated using a first-order Taylor expansion: $\Delta \Gamma_m \approx$
63 $\frac{d\Gamma_m}{dT_s} \Delta T_s$. Substituting this into Eq. (2) gives:

$$\Delta T(p) \approx \Delta T_s + \left(\int_{p_s}^p \frac{d\Gamma_m}{dT_s} dp' \right) \Delta T_s \quad (3)$$

64 Thus the non-monotonicity in moist adiabatic warming is encoded into $d\Gamma_m/dT_s$, the sensitivity
65 of the moist adiabatic lapse rate to surface temperature. Indeed, $d\Gamma_m/dT_s$ is non-monotonic
66 with respect to temperature (dashed line shows the local minima of $d\Gamma_m/dT_s$ in Fig. 2a). Note that
67 $d\Gamma_m/dT_s$ is mostly negative in the troposphere (Fig. 2b). This is consistent with amplified warming
68 aloft because the integral in Eq. (2) is from high to low pressure, which introduces a negative sign.

69 Γ_m is a function of local state variables $\Gamma_m(T, p)$. Thus to make progress in understanding
70 $d\Gamma_m/dT_s$, we must rewrite $d\Gamma_m/dT_s$ in terms of derivatives with respect to the local state variables
71 (T, p) . To do this we first use the chain rule:

$$\frac{d\Gamma_m}{dT_s} = \left(\frac{\partial \Gamma_m}{\partial T} \right)_p \cdot \frac{dT}{dT_s} + \left(\frac{\partial \Gamma_m}{\partial p} \right)_T \cdot \frac{dp}{dT_s} \quad (4)$$

72 The second term $\frac{dp}{dT_s} = 0$ because pressure is the vertical coordinate and is an independent variable.
73 Recognizing that by definition $\Gamma_m = \frac{dT}{dp}$,

$$\frac{d}{dp} \left(\frac{dT}{dT_s} \right) = \left(\frac{\partial \Gamma_m}{\partial T} \right)_p \cdot \frac{dT}{dT_s} \quad (5)$$

74 This is an ordinary differential equation for $\frac{dT}{dT_s}$ as a function of pressure. The solution with the
 75 boundary condition $\frac{dT}{dT_s}(p_s) = 1$, is:

$$\frac{dT}{dT_s} = \exp\left(\int_{p_s}^p \left(\frac{\partial \Gamma_m}{\partial T}\right)_p dp'\right) \quad (6)$$

76 Substituting Eq. (6) back into Eq. (4) gives:

$$\frac{d\Gamma_m}{dT_s} = \left(\frac{\partial \Gamma_m}{\partial T}\right)_p \cdot \exp\left(\int_{p_s}^p \left(\frac{\partial \Gamma_m}{\partial T}\right)_{p'} dp'\right) \quad (7)$$

77 where $(\partial \Gamma_m / \partial T)_p$ is the moist adiabatic lapse rate sensitivity to local temperature T at pressure
 78 level p . The integral describes how a surface temperature perturbation influences Γ_m through the
 79 sum of all Γ_m changes that occur below p .

80 The non-monotonicity can arise from either 1) $(\partial \Gamma_m / \partial T)_p$ being non-monotonic and the integral
 81 acting to amplify it or 2) $(\partial \Gamma_m / \partial T)_p$ being monotonic but sign changes in $(\partial \Gamma_m / \partial T)_p$ leads to
 82 the integral being non-monotonic. Numerical solutions show that $(\partial \Gamma_m / \partial T)_p$ is non-monotonic
 83 (dash-dot line shows the local minima of $d\Gamma_m/dT$ in Fig. 2c), which is further amplified by the
 84 integral term (Fig. 2d).

85 Why is $(\partial \Gamma_m / \partial T)_p$ non-monotonic with T ? To understand this we solve for Γ_m from the first
 86 law of thermodynamics for adiabatic ascent with latent heating assuming the parcel is saturated:

$$c_p dT - \alpha dp + L_v dq_s = 0 \quad (8)$$

87 where c_p is the specific heat capacity of air at constant pressure, α is specific volume, L_v is the
 88 latent heat of vaporization, and q_s is the saturation specific humidity. We assume 1) $c_p \approx c_{pd}$,
 89 neglecting the role of water of all phases on the specific heat capacity and 2) $\alpha \approx \alpha_d = R_d T / p$,
 90 neglecting the virtual effect of vapor on density.

91 Use the chain rule to expand dq_s :

$$dq_s = \left(\frac{\partial q_s}{\partial T}\right)_p dT + \left(\frac{\partial q_s}{\partial p}\right)_T dp \quad (9)$$

Substituting Eq. (9) into Eq. (8) and rearranging gives

$$\left(c_{pd} + L_v \left(\frac{\partial q_s}{\partial T} \right)_p \right) dT = \left(\alpha_d - L_v \left(\frac{\partial q_s}{\partial p} \right)_T \right) dp \quad (10)$$

We can derive closed-form expressions for the q_s derivatives using the Clausius-Clapeyron relation and Dalton's Law. These q_s derivatives describe the role of phase equilibrium shifts in q_s with T and p on the effective heat capacity and specific volume of the air parcel, respectively:

$$c_L \equiv L_v \left(\frac{\partial q_s}{\partial T} \right)_p \approx \frac{L_v^2 q_s}{R_v T^2} \quad (11)$$

$$\alpha_L \equiv -L_v \left(\frac{\partial q_s}{\partial p} \right)_T \approx \frac{L_v q_s}{p} \quad (12)$$

where the approximation arises from assuming saturation vapor pressure $e_s \ll p$.

c_L can be thought of as a latent heat capacity, representing the enhanced thermal inertia due to the fact that latent heating buffers some of the cooling from expansion. Thus c_L acts to increase the heat capacity of the air parcel such that it has an effective heat capacity $c_{pd} + c_L$.

α_L can be thought of as a latent specific volume, representing the enhanced expansion of air with ascent due to the fact that lower pressure shifts the phase equilibrium of water to favor the vapor phase over liquid. Thus α_L acts to increase the volume of air such that it has an effective specific volume $\alpha_d + \alpha_L$.

Now solving for the moist adiabatic lapse rate $\Gamma_m = dT/dp$:

$$\Gamma_m = \frac{dT}{dp} = \frac{\alpha_d + \alpha_L}{c_{pd} + c_L} \quad (13)$$

$$= \Gamma_d \cdot \frac{1 + \frac{\alpha_L}{\alpha_d}}{1 + \frac{c_L}{c_{pd}}} \quad (14)$$

where $\Gamma_d = \alpha_d/c_{pd}$ is the dry adiabatic lapse rate in pressure coordinates and the two non-dimensional terms represent the fractional increase in effective heat capacity and specific volume

107 due to phase equilibrium changes:

$$\tilde{c} = \frac{c_L}{c_{pd}} = \frac{L_v^2 q_s}{c_{pd} R_v T^2} \quad (15)$$

$$\tilde{\alpha} = \frac{\alpha_L}{\alpha_d} = \frac{L_v q_s}{R_d T} = \frac{R_v c_{pd} T}{R_d L_v} \tilde{c} = k \tilde{c} \quad (16)$$

108 Substituting Eq. (15) and Eq. (16) into Eq. (14) gives:

$$\Gamma_m = \Gamma_d \cdot \frac{1 + k \tilde{c}}{1 + \tilde{c}} \quad (17)$$

109 For typical values in Earth's atmosphere ($R_v = 461 \text{ J kg}^{-1} \text{ K}^{-1}$, $R_d = 287 \text{ J kg}^{-1} \text{ K}^{-1}$, $c_{pd} = 1005$
 110 $\text{J kg}^{-1} \text{ K}^{-1}$, $L_v = 2.5 \times 10^6 \text{ J kg}^{-1}$, and $T \in [200, 320] \text{ K}$), the factor $k = \frac{R_v c_{pd} T}{R_d L_v} \in [0.13, 0.21]$.
 111 Thus k is a weak function of temperature and is a quasi-constant of order 10^{-1} . In contrast, \tilde{c} scales
 112 exponentially with temperature (through q_s) and varies from $\tilde{c}(200 \text{ K}) \sim 10^{-4}$ to $\tilde{c}(320 \text{ K}) \sim 10^1$.
 113 Thus the temperature sensitivity of Γ_m is controlled by \tilde{c} . Because Γ_m is bounded between Γ_d
 114 (dry limit, $\tilde{c} \rightarrow 0$) and $k\Gamma_d$ (moist limit, $\tilde{c} \rightarrow \infty$), the magnitude of $\partial\Gamma_m/\partial T$ must peak at some
 115 intermediate \tilde{c} else Γ_m would be unbounded.

116 Where does the magnitude of $\partial\Gamma_m/\partial T$ reach its peak value? To solve this we use the quotient
 117 rule on Eq. (13):

$$\frac{\partial\Gamma_m}{\partial T} = \underbrace{\frac{1}{c_{pd} + c_L} \frac{\partial(\alpha_d + \alpha_L)}{\partial T}}_{\text{latent volume sensitivity}} + \underbrace{\left(-\frac{\alpha_d + \alpha_L}{(c_{pd} + c_L)^2} \frac{\partial c_L}{\partial T} \right)}_{\text{latent heat capacity sensitivity}} \quad (18)$$

118 The latent volume sensitivity varies monotonically with T_s (Fig. 3a, c). The latent heat capacity
 119 sensitivity varies non-monotonically with T_s (Fig. 3b, d). Thus we further decompose the latent
 120 heat capacity sensitivity to probe its origin:

$$-\frac{\alpha_d + \alpha_L}{(c_{pd} + c_L)^2} \frac{\partial c_L}{\partial T} = -\frac{1}{p} \cdot (1 + \tilde{\alpha}) \cdot \frac{R_d}{c_{pd}} \frac{\partial \log c_L}{\partial \log T} \cdot f_d \cdot f_L \quad (19)$$

121 where

$$f_d \equiv c_d / (c_{pd} + c_L) \quad (20)$$

$$f_L \equiv c_L / (c_{pd} + c_L) \quad (21)$$

123 and $f_d + f_L = 1$. f_d and f_L represent the dry and latent fractions of effective heat capacity.

124 Eq. (19) shows the latent heat capacity sensitivity is a product of four terms that vary
 125 monotonically with T . $\tilde{\alpha} = L_v q_s / (\alpha_d p)$ scales exponentially with T through q_s (red line in
 126 Fig. 4a). The fractional change in latent heat capacity to a fractional change in temperature
 127 $\partial \log c_L / \partial \log T = L_v / (R_v T) - 2$ so it weakly decreases with T (blue line in Fig. 4a). The product
 128 of these two terms is weakly non-monotonic in T with a local minimum where $\tilde{\alpha} \approx R_v T / L_v$ (white
 129 line in Fig. 4b). At low T , $\tilde{\alpha}$ is small so the product is dominated by the decrease in $\partial \log c_L / \partial \log T$.
 130 At high T , $\tilde{\alpha}$ is large so the product is dominated by the exponential increase in $\tilde{\alpha}$. However, the
 131 non-monotonicity of these two terms are not the source of the peak in the magnitude of $\partial \Gamma_m / \partial T$,
 132 which requires a local maximum, not a minimum.

133 The dry fraction of effective heat capacity $f_d = c_{pd} / (c_{pd} + c_L)$ logistically decreases with T
 134 because c_{pd} is a constant while latent heat capacity c_L increases exponentially with T through q_s
 135 (blue line in Fig. 4c). The latent fraction of effective heat capacity $f_L = c_L / (c_{pd} + c_L)$ logistically
 136 increases with T (red line in Fig. 4c). The product $f_d \cdot f_L$ is maximized when $f_d = f_L$, or $c_L = c_{pd}$
 137 (black line in Fig. 4d).

138 What is the physical intuition behind the peak at $c_L = c_{pd}$? Recall that c_L quantifies the
 139 enhancement of effective heat capacity due to latent heat of condensation offsetting adiabatic
 140 cooling. The q_s derivative in c_L requires two ingredients: 1) cooling from expansion and 2) water
 141 vapor. f_d and f_L represent the fractional availability of the two ingredients. At low T , condensation
 142 is limited by the availability of water vapor (red line in Fig. 4c). At high T condensation is limited
 143 by adiabatic cooling (blue line in Fig. 4c). The peak in latent heat capacity sensitivity corresponds
 144 to where the availability of cooling and vapor are equally limiting (black line in Fig. 4c). Thus the
 145 non-monotonicity in $\partial \Gamma_m / \partial T$ and moist adiabatic warming arises from the competition between
 146 the two limiting factors of condensation.

147 How well does the condition $c_L = c_{pd}$ capture the actual peak in $\partial \Gamma_m / \partial T$? The the-
 148 ory slightly overpredicts the T_s where the magnitude of $\partial \Gamma_m / \partial T$ peaks (compare solid and
 149 dash-dot lines in Fig. 5). This error is due to the weak non-monotonicity in the product
 150 $(1 + \tilde{\alpha}) R_d / c_{pd} \partial \log(c_L) / \partial \log(T)$ which decreases with pressure (Fig. 4b). The error maximizes
 151 at the surface where the theory predicts a peak T_s that is 1.6 K warmer than the true peak T_s .

152 The error in T_s predicted by the theory and the true peak of Γ_m/dT_s grows with height because
 153 the integral term in Eq. (7) amplifies the error in $\partial\Gamma_m/\partial T$ at each level below. This error maximizes
 154 at 420 hPa where $c_L = c_{pd}$ predicts a peak T_s that is 2.0 K warmer than the true peak T_s (compare
 155 solid and dashed lines in Fig. 5). This error is further compounded for T_s corresponding to the peak
 156 of moist adiabatic warming ΔT (Eq. 3), leading to a maximum error of 6.6 K at 420 hPa (compare
 157 solid and dotted lines in Fig. 5). Thus the condition $c_L = c_{pd}$ provides a useful first-order estimate
 158 of T_s where moist adiabatic warming peaks. Importantly the theory successfully captures the shift
 159 to warmer peak T_s with height, which is due to the fact that temperature decreases with height and
 160 thus the transition from the vapor limited to cooling limited regime occurs at a warmer surface
 161 temperature with height.

178 3. Implications of non-monotonicity in moist adiabatic warming on convection

179 The non-monotonic warming of a moist adiabat has implications for the dynamics of convection.
 180 For example, Romps (2016) showed that parcel buoyancy is a non-monotonic function of surface
 181 temperature. Specifically the criterion where B peaks is $\beta = 2c_{pd}$ where

$$\beta = c_{pd} + L_v \frac{\partial q_s}{\partial T} = c_{pd} + c_L \quad (22)$$

182 Thus the criterion that maximizes B is equivalent to where moist adiabatic warming peaks, $c_{pd} = c_L$.
 183 Below, we show this is true if the entrainment parameter $a = PE\epsilon/g^1$ is small and derive a more
 184 general criterion that maximizes B .

185 Buoyancy B is the normalized virtual temperature (or equivalently, density) difference between
 186 the rising parcel $T_{v,p}$ and the environment $T_{v,e}$. Here we neglect the virtual effects of water and we
 187 use standard temperature:

$$B \approx \frac{g}{T_e} (T_p - T_e) \quad (23)$$

188 As before, we express temperature profiles in terms of T_s and the integral of their respective lapse
 189 rates. We assume the parcel follows a moist adiabatic lapse rate, Γ_m , while the environment follows

¹ PE is precipitation efficiency, ϵ is the fractional entrainment rate, and g is gravitational acceleration. See Romps (2016) for the derivation of the entraining plume model.

fig-2.png

FIG. 2. (a) The sensitivity of the moist adiabatic lapse rate to surface temperature, $d\Gamma_m/dT_s$, varies non-monotonically with surface temperature. (b) $d\Gamma_m/dT_s$ has a local minimum across surface temperature. A minimum in $d\Gamma_m/dT_s$ corresponds to a maximum in moist adiabatic warming (Fig. 1b) because the integral bounds in Eq. 3 decreases from p_s to p , which introduces a negative sign. (c) The sensitivity of the moist adiabatic lapse rate to the local temperature at pressure p , $\partial\Gamma_m/\partial T$, also varies non-monotonically with surface temperature. (d) The integral term in Eq. (7) amplifies the non-monotonicity of $\partial\Gamma_m/\partial T$. (a) is the product of (c) and (d).

an entraining lapse rate, Γ_e .

$$T_p = T_s + \int_{p_s}^p \Gamma_m(p') dp' \quad (24)$$

$$T_e = T_s + \int_{p_{s1}}^p \Gamma_e(p') dp' \quad (25)$$

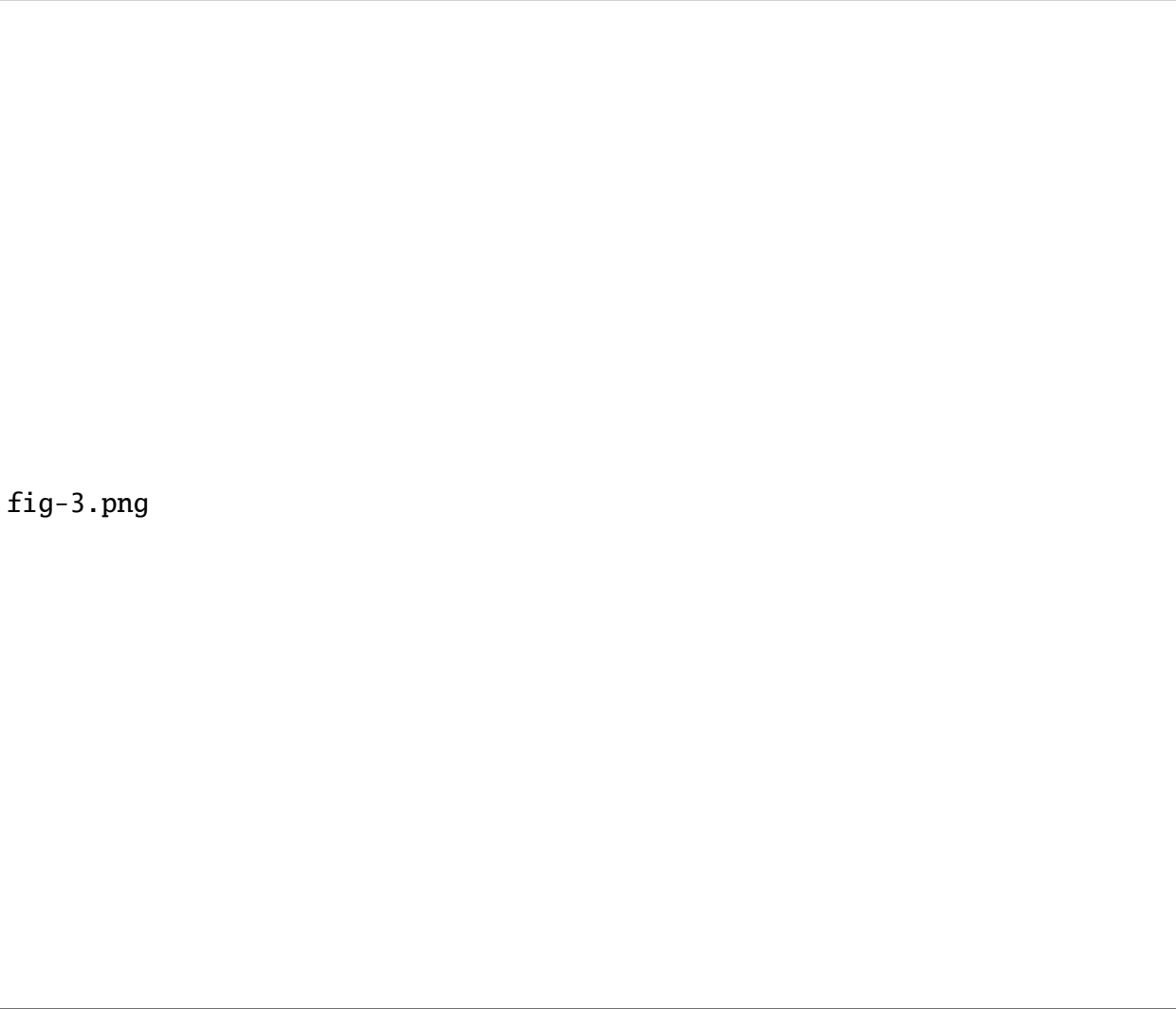


fig-3.png

FIG. 3. Warming is decomposed into contributions from the Cooling Term and the Pressure Term. (a) The vertical profile of the warming contribution from the Cooling Term for select T_s . (b) The warming contribution from the Cooling Term at fixed heights as a function of surface temperature. This term provides a warming effect that increases monotonically with temperature. (c) The vertical profile of the relative cooling contribution from the Pressure Term. (d) The relative cooling from the Pressure Term at fixed heights. Both the Cooling and Pressure terms become stronger as the surface temperature increases.

Substituting Eq. (24) and (25) into the definition of buoyancy Eq. (23) yields:

$$B \approx \frac{g}{T_e} \int_{p_s}^p \delta\Gamma dp' \quad (26)$$

fig-4.png

FIG. 4. The (a) Cooling Prefactor, $\Gamma_m L_v / (R_v T^2)$, and (b) Pressure Prefactor, $g / (R_d T_v)$, as a function of height and surface temperature. The Cooling Prefactor weakens strongly with temperature due to its $1/T^2$ dependence. In contrast, the Pressure Prefactor weakens more slowly due to its $1/T_v$ dependence.

where $\delta\Gamma = \Gamma_e - \Gamma_m$. We use the same entraining plume model as in Romps (2016) but express the lapse rate in pressure coordinates:

$$\Gamma_e = \Gamma_d \cdot \frac{(1+a)\alpha_d + \alpha_L}{(1+a)c_{pd} + c_L} \quad (27)$$

Substituting Eq. (13) and (27) into Eq. (26) and simplifying gives:

$$B = \frac{g}{T_e} \int_{p_s}^p \Gamma_d \cdot \frac{a(1-k)\tilde{c}}{(1+a+\tilde{c})(1+\tilde{c})} dp' \quad (28)$$

If we assume that a does not vary with T_s , T_e increases monotonically with T_s at all p . The origin of the non-monotonicity of B must be in the integrand, $\delta\Gamma$. B depends on T primarily through \tilde{c} , which scales exponentially with T through q_s , whereas Γ_d and k are linear functions of T . In the limit of $\tilde{c} \rightarrow 0$ (cold and dry), $\delta\Gamma$ scales as \tilde{c} , which increases with T . In the limit of $\tilde{c} \rightarrow \infty$ (warm and humid), $\delta\Gamma$ scales as \tilde{c}^{-1} , which decreases with increasing T . Thus the integrand maximizes at some intermediate \tilde{c} .

To solve for the condition that maximizes buoyancy we solve for the \tilde{c} derivative of the integrand $\delta\Gamma$ in Eq. (28) and set it to zero:

$$\frac{d}{d\tilde{c}} \left(\Gamma_d \cdot \frac{a(1-k)\tilde{c}}{(1+a+\tilde{c})(1+\tilde{c})} \right) = 0 \quad (29)$$

If we assume that a , k , and Γ_d do not vary with T , the solution to Eq. (29) is

$$\tilde{c}_{\text{peak}} = \sqrt{1+a} \quad (30)$$

Thus the condition that maximizes buoyancy is $c_L = \sqrt{1+a}c_{pd}$. In the limit of weak entrainment $a \rightarrow 0$, this reduces to $c_L = c_{pd}$. In the presence of entrainment, buoyancy peaks at a higher c_L and thus higher T_s all else equal. Entrainment reduces the latent heat released by the cooling parcel given the same q_s so it shifts the critical point that separates the vapor limited and cooling limited regimes toward higher q_s .

How important is the factor $\sqrt{1+a}$? For an entrainment rate representative of Earth's current climate $a = 0.2$, the difference in peak T_s that corresponds to $c_L = c_{pd}$ and $c_L = \sqrt{1+a}c_{pd}$ are < 1.49 K (compare red and solid black line in Fig. 6a). This difference decreases with height and becomes negligibly small around the tropopause (e.g., 0.33 K at $p = 100$ hPa), which explains why the criteria $c_L = c_{pd}$ works well for explaining the non-monotonicity of CAPE (Romps 2016). However, for stronger entrainment rates and for understanding the non-monotonicity of buoyancy

215 in the lower troposphere the factor $\sqrt{1+a}$ can be important (e.g., 4.38 K for $a = 0.7$ at the surface;
 216 compare red and solid black line in Fig. 6b).

217 How well do these criteria capture the T_s that maximizes buoyancy across the troposphere? We
 218 will first focus on $\delta\Gamma$, i.e. the integrand in Eq. (26). For $a = 0.2$ both criteria capture the T_s
 219 that corresponds to the peak in $\delta\Gamma$ well (< 1.39 K for $c_L = \sqrt{1+a}c_{pd}$, < 2.87 K for $c_L = c_{pd}$,
 220 compare red and solid black line to dashed line in Fig. 6a). The small error arises even for the
 221 $c_L = \sqrt{1+a}c_{pd}$ criterion because $\Gamma_d(1-k)$ is weakly non-monotonic with T (Γ_d increases with T
 222 and $(1-k)$ decreases with T), which we ignored in order to analytically solve Eq. (29). This error
 223 is amplified as we integrate $\delta\Gamma$ to obtain buoyancy Eq. (26) because the errors in the location of
 224 peak $\delta\Gamma$ from each level below accumulates for the location of peak B compare red and solid black
 225 line to dotted line in Fig. 6a).

226 For a higher entrainment parameter $a = 0.7$ the importance of the factor $\sqrt{1+a}$ becomes clear.
 227 The error in T_s that corresponds to the peak in $\delta\Gamma$ is < 3.39 K for the $c_L = \sqrt{1+a}c_{pd}$ criterion
 228 compared to < 5.83 K for the $c_L = c_{pd}$ criterion (compare red and solid black line to dashed line
 229 in Fig. 6b). The error in T_s that corresponds to the peak in buoyancy is surprisingly lower for
 230 the $c_L = c_{pd}$ criterion (< 3.37 K) compared to the $c_L = \sqrt{1+a}c_{pd}$ criterion (< 4.66 K, compare
 231 red and solid black lines to dotted black line in Fig. 6b). This is because $c_L = c_{pd}$ underpredicts
 232 T_s for peak B in the lower troposphere, which offsets the growth of the larger error in peak $\delta\Gamma$
 233 (compare solid black and dotted lines in Fig. 6b). While the criteria $c_L = c_{pd}$ may provide a better
 234 estimate of peak buoyancy in some cases, it doesn't do so for the right reasons. For example the
 235 criteria $c_L = c_{pd}$ predicts no shift in T_s that maximizes B to perturbations in a while the criterion
 236 $c_L = \sqrt{1+a}c_{pd}$ captures the shift in peak $\delta\Gamma$ and B toward warmer T_s with increasing entrainment
 237 (Fig. 6c).

238 This non-monotonic behavior of buoyancy extends to the strength of the convective updraft. We
 239 model the updraft's specific kinetic energy, $\frac{1}{2}w^2$, using Eq. (1) from Del Genio et al. (2007):

$$\frac{d}{dz} \left(\frac{1}{2} w^2 \right) = a' B(z) - (1 + b') \epsilon(z) w^2 \quad (31)$$

240 where a' and b' are dimensionless constants. We use $a' = 1/6$ and $b' = 2/3$ following Del Genio
 241 et al. (2007). $\epsilon(z)$ is the fractional entrainment rate, which is calculated following Eq. (3) in Romps

(2016) with entrainment parameter $a = 0.2$ and precipitation efficiency $PE = 0.35$. Since $w(z)$ is determined by the integral of the net force, which includes buoyancy, we expect the non-monotonic dependence on T_s extends to the vertical velocity profile as well.

Numerically integrating Eq. (31) confirms this expectation. The resulting vertical velocity varies non-monotonically with T_s (Fig. 7b). This leads $w(z)$ becoming more top-heavy with warming, i.e. w decreases in the lower troposphere and increases in the upper troposphere (Fig. 7a).

Are these findings relevant to Earth's atmosphere, where convection is not strictly moist adiabatic and vertical velocity is subject to details and constraints not considered here such as cloud microphysics and radiative cooling? To test this we analyzed output from a set of 9 convective-resolving models simulating radiative convective equilibrium in a 100 km x 100 km domain from the RCEMIP project (Wing et al. 2018). We look at the mean vertical velocity profiles for w exceeding the 99.9th percentile at each height level. The 99.9th percentile corresponds to the fastest 1000 samples of w per level per model. We focus on strong convective updrafts because the buoyancy is highest for those parcels that are closest to the moist adiabat.

The vertical velocity profiles from the RCEMIP simulations show diverse $w_{>99.9}$ responses to variations in surface temperature (295, 300, and 305 K, see Fig. 8). Some models exhibit a clear top-heavy shift in $w_{>99.9}$ with warming (e.g., CM1, DAM, UCLA-CRM, UKMO, WRF) accompanied by a decrease in $w_{>99.9}$ in the lower troposphere that is qualitatively consistent with the moist adiabatic theory (Fig. 7a). SAM shows a top-heavy shift in $w_{>99.9}$ without a clear decrease in $w_{>99.9}$ in the lower troposphere. In the remaining models the $w_{>99.9}$ response exhibits non-monotonicity with T_s but the peak $w_{>99.9}$ does not necessarily increase. For example DALES and SCALE predict a non-monotonic response in $w_{>99.9}$ with T_s at $z \approx 8$ km but the peak $w_{>99.9}$ weakens from $T_s = 300$ to 305 K. MesoNH also predicts a decrease in peak $w_{>99.9}$ from $T_s = 300$ K to 305 K but predicts a non-monotonic response in $w_{>99.9}$ with T_s at $z \approx 3$ km, much lower than in DALES and SCALE. The diversity in responses likely arises from differences in model details and emergent behavior such as convective organization that influence convective dynamics beyond the thermodynamic processes considered here. Nonetheless, the presence of non-monotonicity and a top-heavy shift in several models suggest that the implications of non-monotonicity in moist adiabatic warming on convective dynamics may be playing a role in shaping the response of convective updrafts in the real atmosphere.

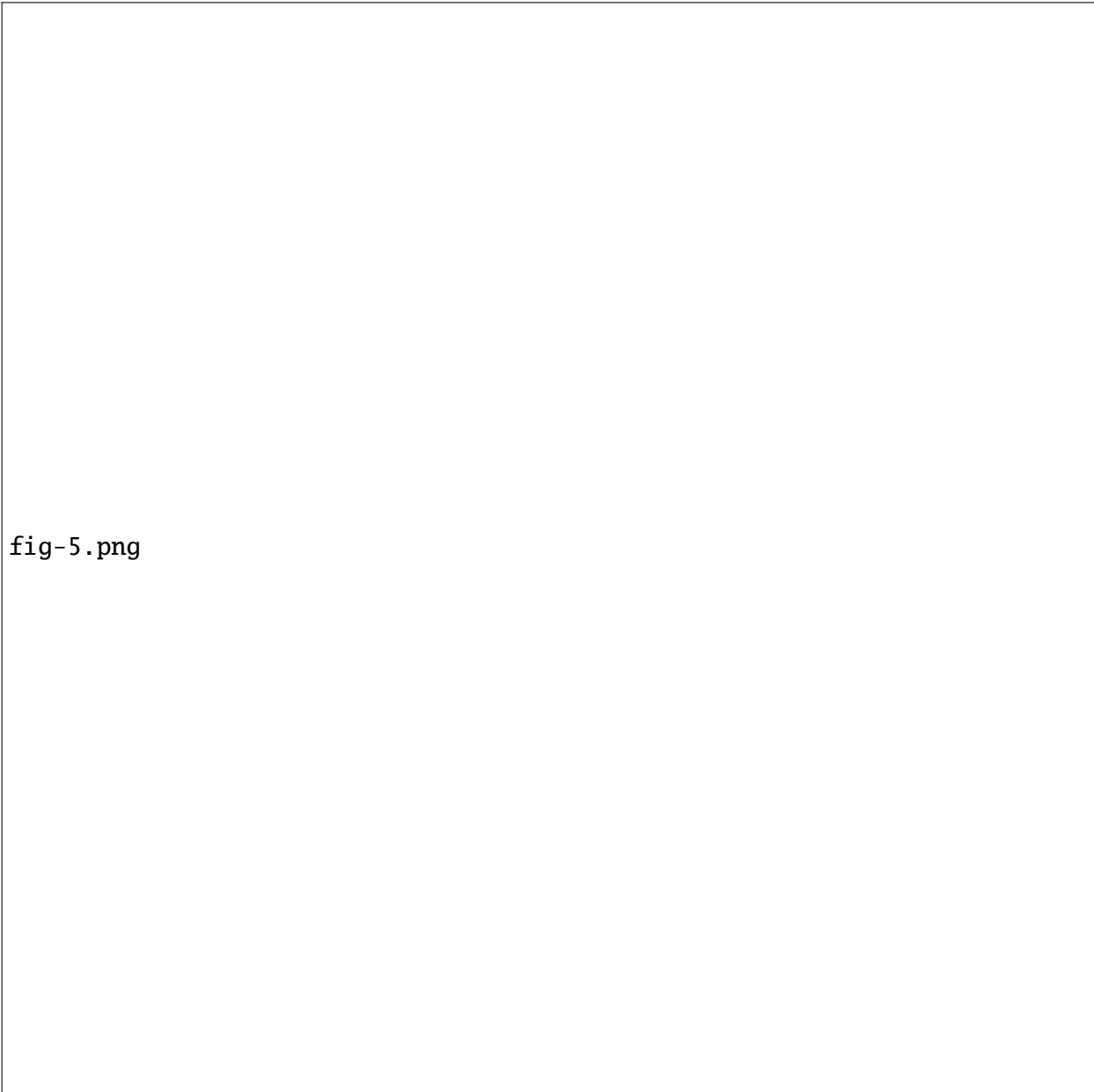


fig-5.png

272 FIG. 5. (a) Vertical profiles of buoyancy for an undiluted parcel ascending through an environment set by an
273 entraining plume, calculated for several surface temperatures. (b) Buoyancy at fixed heights as a function of
274 surface temperature. The entraining environmental profile follows Romps (2016).

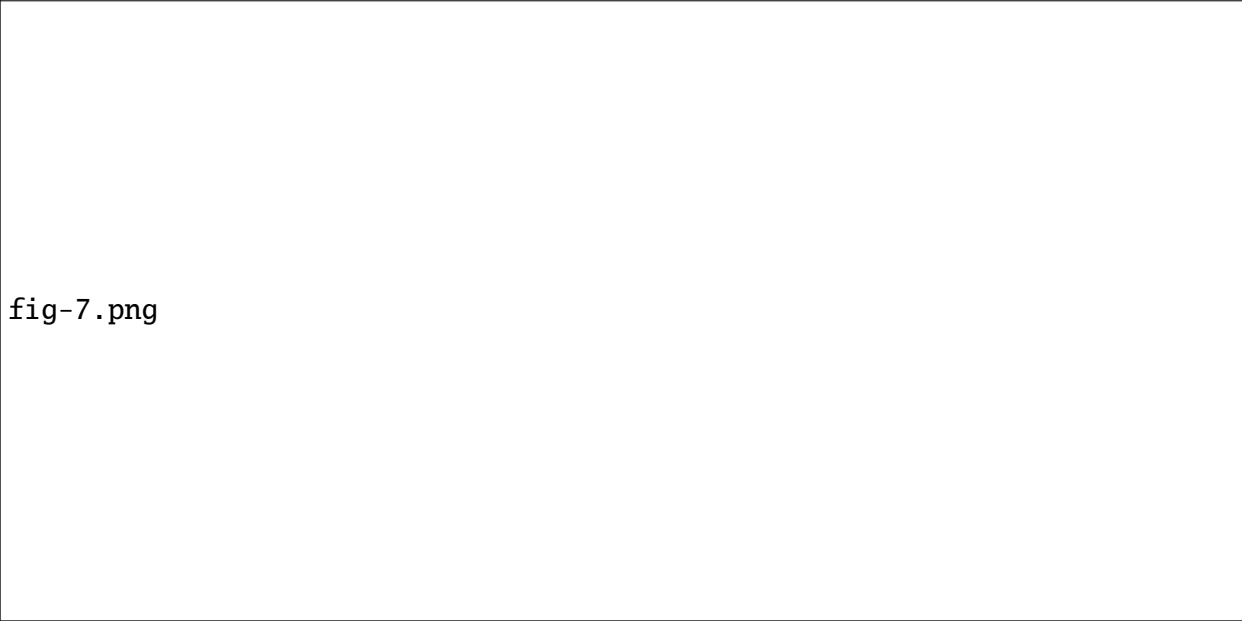


fig-7.png

279 FIG. 7. (a) Vertical profiles of updraft velocity, calculated by numerically integrating Eq. (31) using the total
280 buoyancy from Fig. 5. (b) Updraft velocity at fixed heights as a function of surface temperature. The velocity
281 exhibits a clear non-monotonic dependence on surface temperature, consistent with the behavior of buoyancy.

4. Summary and Discussion

This paper presents a thermodynamic explanation for the non-monotonicity of moist adiabatic warming. The non-monotonicity arises through

Our findings on buoyancy complement the work of Romps (2016), who first explained the non-monotonicity of CAPE. The two studies offer different but complementary insights. Romps (2016) focused on explaining the non-monotonicity of buoyancy at the tropopause as a proxy for CAPE. Here, we focus on explaining the non-monotonicity of buoyancy at any fixed height. We also provide a different perspective on the source of non-monotonicity that arises from the competition in the sensitivity of a Cooling Term that favors condensation and a Pressure Term, driven by decreasing ambient pressure, that opposes it.

The non-monotonicity of moist adiabatic warming may have additional implications for climate, such as the organization of convection and the large-scale circulation response to warming. The non-monotonicity of moist adiabatic warming would drive a non-monotonic change in the meridional and zonal temperature gradients. This could serve as a thermodynamically driven hypothesis for understanding state dependence in the response of Hadley and Walker Cells to warming.

Acknowledgments. I thank Andrew Williams, Jiawei Bao, Jonah Bloch-Johnson, Martin Singh, Stephen Po-Chedley, Nadir Jeevanjee, and two anonymous reviewers for helpful discussions and feedback on the manuscript.

Data availability statement. All scripts used for analysis and plots in this paper are available at <https://github.com/omiyawaki/miyawaki-2025-nonmonotonic-moist-adiabat>. They will also be archived on Zenodo upon publication.

APPENDIX A

Calculation of Moist Adiabatic Profiles

The moist adiabatic profiles are calculated numerically by assuming that saturation moist static energy h is conserved, where:

$$h = c_p T + gz + L_v q_s \quad (\text{A1})$$

Here, T is temperature, z is height, q_s is the saturation specific humidity, g is the acceleration due to gravity, c_p is the specific heat of dry air at constant pressure, and L_v is the latent heat of




fig-8.png

FIG. 8. The total vertical velocity is decomposed to show the influence of the Cooling and Pressure terms. (a,b) The velocity profile resulting from the positive buoyancy of the Cooling Term alone. (c,d) The effect of the Pressure Term on velocity, calculated as the residual between the total velocity and the velocity from the Cooling Term.

313 vaporization. All thermodynamic constants are defined in Table A1. Saturation vapor pressure is
314 calculated using Eq. (10) in Bolton (1980).

315 The calculation proceeds in discrete vertical steps of $\Delta p = 50$ Pa). For a given surface temperature
316 (T_s) and surface pressure (p_s), h is first calculated at the surface ($z = 0$) and is held constant over
317 height. At each subsequent pressure step p_{i+1} , the height z_{i+1} is calculated using hydrostatic
318 balance. Then, a numerical root-finding algorithm (scipy.optimize.root_scalar with the Brentq
319 method) is used to find the temperature T_{i+1} that satisfies the condition that the h at $(T_{i+1}, p_{i+1}, z_{i+1})$
320 is equal to the surface h .

321 To demonstrate that the non-monotonic warming is independent of the vertical coordinate, the
322 results are also presented in height coordinates (Fig. A1). These profiles are obtained by following
323 the same calculation as above except stepping in uniform intervals $\Delta z = 100$ m. The pressure p_{i+1}
324 at height z_{i+1} is calculated using hydrostatic balance.

fig-a1.png

325 FIG. A1. The moist adiabatic warming response to a 4 K surface warming in pressure coordinates. (a) Vertical
326 profiles of the temperature response (ΔT) as a function of pressure for surface temperatures (T_s) 280, 290, 300,
327 310, and 320 K. (b) The warming (ΔT) at 5 km, 10 km, 15 km, and 20 km as a function of T_s . The non-monotonic
328 behavior seen in height coordinates (Fig. 1c) is also evident in pressure coordinates.

APPENDIX B

TABLE A1. Thermodynamic constants used in the calculation of moist adiabatic profiles.

Symbol	Description	Value	Units
g	Acceleration due to gravity	9.81	m s^{-2}
c_p	Specific heat of dry air	1005.7	$\text{J kg}^{-1} \text{K}^{-1}$
R_d	Gas constant for dry air	287.05	$\text{J kg}^{-1} \text{K}^{-1}$
R_v	Gas constant for water vapor	461.5	$\text{J kg}^{-1} \text{K}^{-1}$
ϵ	Ratio of gas constants (R_d/R_v)	0.622	dimensionless
p_s	Surface pressure	1000	hPa
L_v	Latent heat of vaporization	2.501×10^6	J kg^{-1}

Effect of Latent Heat of Fusion on Moist Adiabatic Warming

We assess how latent heat of fusion influences the non-monotonicity of moist adiabatic warming. We follow the IFS Cycle 40 approximations as summarized by Flannaghan et al. (2014). The fraction of liquid water α varies with T as follows:

$$\alpha(T) = \begin{cases} 0, & T \leq T_{\text{ice}}, \\ \left(\frac{T - T_{\text{ice}}}{T_0 - T_{\text{ice}}} \right)^2 & T_{\text{ice}} < T < T_0, \\ 1 & T \geq T_0, \end{cases} \quad (\text{B1})$$

where $T_{\text{ice}} = 253.15 \text{ K}$ and $T_0 = 273.15 \text{ K}$. Thus all condensate is ice below 253.15 K, all condensate is liquid above 273.15 K, and a quadratic transition occurs in between.

The saturation vapor pressure e_s is the weighted average over liquid (e_ℓ) and ice (e_i):

$$e_s = \alpha e_\ell + (1 - \alpha) e_i \quad (\text{B2})$$

The saturation vapor pressure over liquid and ice is:

$$e_{\ell,i}(T) = a_1 \exp \left(a_3 \frac{T - T_0}{T - a_4} \right) \quad (\text{B3})$$

where over liquid $a_1 = 611.21 \text{ Pa}$, $a_3 = 17.502$, $a_4 = 32.19 \text{ K}$ (Buck 1981) and over ice $a_1 = 611.21 \text{ Pa}$, $a_3 = 22.587$, $a_4 = -0.7 \text{ K}$ (Alduchov and Eskridge 1996).

The effective latent heat of vaporization $L_e(T)$ includes both condensation and fusion:

$$L_e(T) = L_v + (1 - \alpha)L_f \quad (\text{B4})$$

where $L_f = 0.334 \times 10^6 \text{ J kg}^{-1}$ is the latent heat of fusion.

Moist adiabats are obtained by solving for T that conserves moist static energy with the effective latent heat L_e :

$$h = c_{pd}T + gz + L_e q_s \quad (\text{B5})$$

The vertical profiles of warming ΔT and the warming at fixed pressure levels versus surface temperature exhibit similar non-monotonic behavior to the case without fusion (compare Fig. 1 and B1). Latent heat of fusion introduces a secondary local maximum in the warming in the mid troposphere (500 hPa) due to the additional energy release from fusion. When the secondary peak is to the right of the primary peak the T_s corresponding to peak warming shifts to colder T_s with fusion (points below the 1:1 line in Fig. B1). As the secondary peak overlaps with the primary peak the T_s corresponding to peak warming shifts to warmer T_s with fusion (points above the 1:1 line in Fig. B1). This effect is greatest (6.03 K) at 727 hPa. Since fusion represents a secondary effect and complicates analytical treatment, we neglect it for the rest of the paper.

APPENDIX C

Effect of Saturation Vapor Pressure Formula on Moist Adiabatic Warming

The calculation of moist adiabatic warming profiles depends on the choice of the saturation vapor pressure formula. To assess the sensitivity of surface temperatures associated with peak moist adiabatic warming to different formula we test three formula: Bolton (1980), Goff-Gratch (List 1949), and Murphy and Koop (2005).

The Bolton (1980) formula is:

$$e_s = 6.112 \exp\left(\frac{17.67(T - 273.15)}{T - 29.65}\right) \quad [\text{hPa}], \quad (\text{C1})$$

The Goff-Gratch formula is:

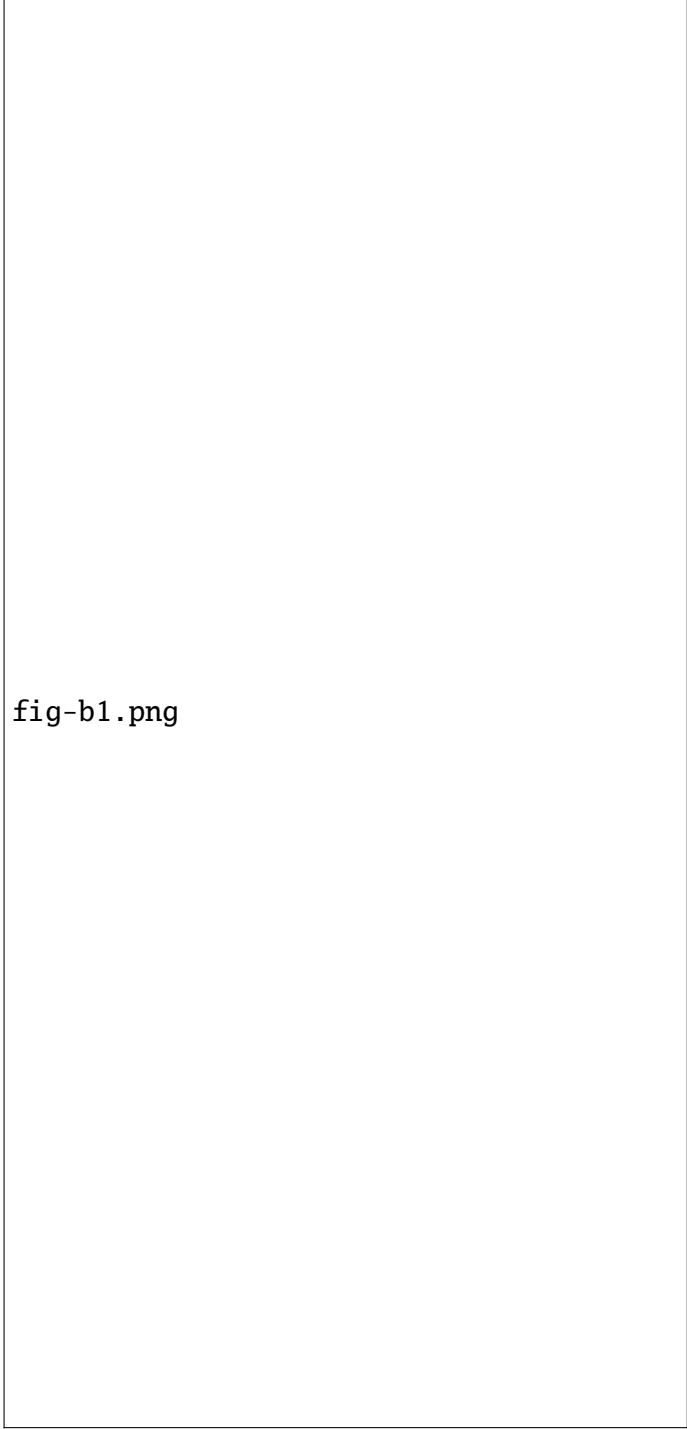


fig-b1.png

FIG. B1. The moist adiabatic warming response to a 4 K surface warming with latent heat of fusion. (a) Vertical profiles of the temperature response (ΔT) as a function of pressure for surface temperatures (T_s) of 280, 290, 300, 310, and 320 K. (b) The warming (ΔT) at fixed pressure levels of 500, 400, 300, and 200 hPa as a function of T_s . (c) T_s corresponding to peak warming with and without fusion.

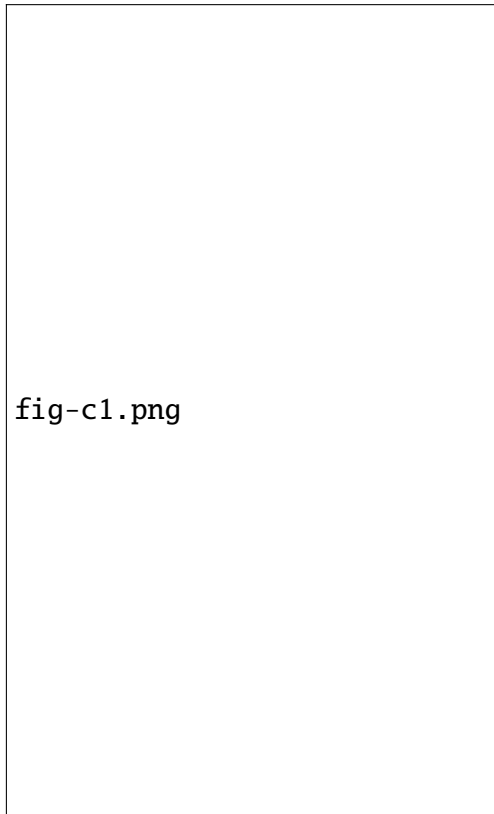
$$\begin{aligned}
\log_{10} e_w = & -7.90298 \left(\frac{373.16}{T} - 1 \right) + 5.02808 \log_{10} \left(\frac{373.16}{T} \right) \\
& - 1.3816 \times 10^{-7} \left(10^{11.344(1-T/373.16)} - 1 \right) \\
& + 8.1328 \times 10^{-3} \left(10^{-3.49149(373.16/T-1)} - 1 \right) \\
& + \log_{10}(1013.246) \quad [\text{hPa}] \quad (\text{C2})
\end{aligned}$$

The Murphy and Koop (2005) formula is:

$$\begin{aligned}
\ln e_w = & 54.842763 - \frac{6763.22}{T} - 4.210 \ln T + 0.000367T \\
& + \tanh(0.0415(T - 218.8)) \left(53.878 - \frac{1331.22}{T} - 9.44523 \ln T + 0.014025T \right) \quad [\text{Pa}], \quad (\text{C3})
\end{aligned}$$

where T is in Kelvin for all 3 formula.

Bolton (1980) is sufficiently accurate for the purposes of evaluating the T_s that leads to maxima in moist adiabatic warming (Fig. C1). The differences in peak T_s across the three saturation vapor pressure formula are small, with the largest deviation being 0.27 K between Bolton and Goff-Gratch and 0.34 K between Bolton and Murphy-Koop. Thus we use Bolton (1980) for the rest of the paper.



371 FIG. C1. (a) T_s corresponding to peak warming using Bolton (1980) and Goff-Gratch saturation vapor pressure
372 formula. (b) Same as (a) but comparing Bolton (1980) and Murphy and Koop (2005).

References

- Alduchov, O. A., and R. Eskridge, 1996: Improved magnus form approximation of saturation vapor pressure. *Journal of Applied Meteorology*, **35** (4), 601–609.
- Bolton, D., 1980: The computation of equivalent potential temperature. *Mon. Weather Rev.*, **108** (7), 1046–1053.
- Buck, A. L., 1981: New equations for computing vapor pressure and enhancement factor. *Journal of Applied Meteorology and Climatology*, **20** (12), 1527–1532.
- Del Genio, A. D., M.-S. Yao, and J. Jonas, 2007: Will moist convection be stronger in a warmer climate?: CONVECTION STRENGTH IN a WARMER CLIMATE. *Geophys. Res. Lett.*, **34** (16).
- Emanuel, K. A., 1994: *Atmospheric Convection*. Oxford University Press.
- Flannaghan, T. J., S. Fueglistaler, I. M. Held, S. Po-Chedley, B. Wyman, and M. Zhao, 2014: Tropical temperature trends in atmospheric general circulation model simulations and the impact of uncertainties in observed SSTs. *Journal of Geophysical Research, D: Atmospheres*, **119** (23), 13,327–13,337.
- Hansen, J., A. Lacis, D. Rind, G. Russell, P. Stone, I. Fung, R. Ruedy, and J. Lerner, 1984: Climate sensitivity: Analysis of feedback mechanisms. *Climate Processes and Climate Sensitivity*, American Geophysical Union (AGU), 130–163.
- Held, I. M., 1993: Large-scale dynamics and global warming. *Bull. Am. Meteorol. Soc.*, **74** (2), 228–242.
- Held, I. M., and K. M. Shell, 2012: Using relative humidity as a state variable in climate feedback analysis. *Journal of climate*, **25** (8), 2578–2582.
- Held, I. M., and B. J. Soden, 2000: Water vapor feedback and global warming. *Annual review of energy and the environment*, **25** (1), 441–475.
- Levine, X. J., and W. R. Boos, 2016: A mechanism for the response of the zonally asymmetric subtropical hydrologic cycle to global warming. *J. Clim.*, **29** (21), 7851–7867.
- List, R. J., 1949: Smithsonian meteorological tables. *Smithsonian miscellaneous collections*, **114**, 1–521.

- 400 Miyawaki, O., Z. Tan, T. A. Shaw, and M. F. Jansen, 2020: Quantifying key mechanisms that
 401 contribute to the deviation of the tropical warming profile from a moist adiabat. *Geophys. Res.*
 402 *Lett.*, **47** (20), e2020GL089136.
- 403 Murphy, D. M., and T. Koop, 2005: Review of the vapour pressures of ice and supercooled water
 404 for atmospheric applications. *Quarterly journal of the Royal Meteorological Society. Royal*
 405 *Meteorological Society (Great Britain)*, **131** (608), 1539–1565.
- 406 Neelin, J. D., and I. M. Held, 1987: Modeling tropical convergence based on the moist static energy
 407 budget. *Mon. Weather Rev.*, **115** (1), 3–12.
- 408 O’Gorman, P. A., 2015: Precipitation extremes under climate change. *Current climate change*
 409 *reports*, **1** (2), 49–59.
- 410 Romps, D. M., 2016: Clausius–Clapeyron scaling of CAPE from analytical solutions to RCE. *J.*
 411 *Atmos. Sci.*, **73** (9), 3719–3737.
- 412 Santer, B. D., and Coauthors, 2005: Amplification of surface temperature trends and variability in
 413 the tropical atmosphere. *Science*, **309** (5740), 1551–1556.
- 414 Seeley, J. T., N. Jeevanjee, and D. M. Romps, 2019: FAT or FiTT: Are anvil clouds or the
 415 tropopause temperature invariant? *Geophysical research letters*, **46** (3), 1842–1850.
- 416 Vallis, G. K., P. Zurita-Gotor, C. Cairns, and J. Kidston, 2015: Response of the large-scale structure
 417 of the atmosphere to global warming. *Quart. J. Roy. Meteor. Soc.*, **141** (690), 1479–1501.
- 418 Wing, A. A., K. A. Reed, M. Satoh, B. Stevens, S. Bony, and T. Ohno, 2018: Radiative–convective
 419 equilibrium model intercomparison project. *Geoscientific Model Development*, **11** (2), 793–813.